

1 **Update on the Temperature Corrections of Global Air-Sea CO₂ Flux**
2 **Estimates**

3 **Yuanxu Dong^{1,2}, Dorothee C. E. Bakker^{1*}, Thomas G. Bell², Boyin Huang³, Peter**
4 **Landschützer⁴, Peter S. Liss¹, Mingxi Yang²**

5 ¹Centre for Ocean and Atmospheric Sciences, School of Environmental Sciences, University
6 of East Anglia, Norwich, UK

7 ²Plymouth Marine Laboratory, Prospect Place, Plymouth, UK

8 ³National Centers for Environmental Information, National Oceanic and Atmospheric
9 Administration, Asheville, NC, USA

10 ⁴Max Planck Institute for Meteorology, Hamburg, Germany

11

12 *Correspondence to:* Yuanxu Dong (Yuanxu.Dong@uea.ac.uk)

13 *Co-corresponding author: Dorothee C. E. Bakker (D.Bakker@uea.ac.uk)

14

15 **Key points:**

- 16
- 17 • The impact of the warm bias in an *in-situ* SST dataset and the cool skin effect on air-
18 sea CO₂ flux estimates are re-visited
 - 19 • The updated temperature corrections imply a smaller increase in net ocean CO₂ uptake
20 (~35%) compared to a previous study (~50%)
 - 21 • The revised observation-based CO₂ flux agrees well with the independent ocean carbon
22 inventory

23 **Abstract**

24 The oceans are a major carbon sink. Sea surface temperature (SST) is a crucial variable in the
25 calculation of the air-sea carbon dioxide (CO₂) flux from surface observations. Any bias in the
26 SST or any upper ocean vertical temperature gradient (e.g., the cool skin effect) potentially
27 generates a bias in the CO₂ flux estimates. A recent study suggested a substantial increase (~50%
28 or ~0.9 Pg C yr⁻¹) in the global ocean CO₂ uptake due to this temperature effect. Here, we use
29 a gold standard buoy SST dataset as the reference to assess the accuracy of *in-situ* SST used
30 for flux calculation. A physical model is then used to estimate the cool skin effect, which varies
31 with latitude. The bias-corrected SST (assessed by buoy SST) coupled with the physics-based
32 cool skin correction increases the average ocean CO₂ uptake by ~35% (0.6 Pg C yr⁻¹) for 1982
33 to 2020, which is significantly smaller than the previous correction. After these temperature
34 considerations, we estimate an average net ocean CO₂ uptake of 2.2 ± 0.4 Pg C yr⁻¹ for 1994 to
35 2007 based on an ensemble of surface observation-based flux estimates, in line with the
36 independent interior ocean carbon storage estimate corrected for the river induced natural
37 outgassing flux (2.1 ± 0.4 Pg C yr⁻¹).

38

39 **Plain Language Summary**

40 The global oceans play a major role in taking up carbon dioxide (CO₂) released by human
41 activity from the atmosphere. Accurate sea surface temperature (SST) measurements and
42 quantification of any upper ocean temperature gradients (e.g., cool skin effect) are critical for
43 ocean CO₂ uptake estimates. We determine a slight warm bias in the SST dataset used for CO₂
44 flux calculation by utilizing a gold standard reference buoy SST dataset. We then derive a
45 physics-based temperature correction for the ubiquitous cool skin effect on the ocean surface.
46 The temperature revised CO₂ flux bridges the gap between estimates from the surface
47 observation-based air-sea CO₂ fluxes and from the independent ocean carbon inventory.

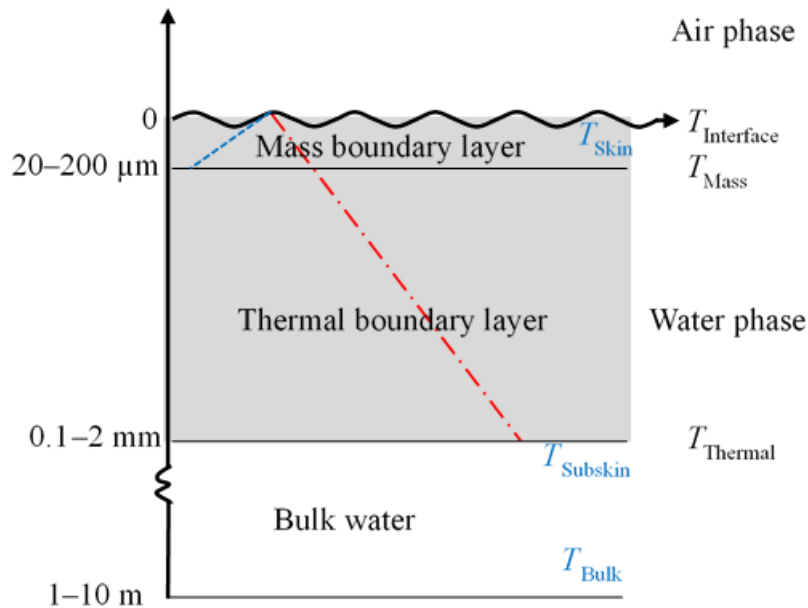
48

49

50 **1 Introduction**

51 Since the Industrial Revolution, humans have emitted large amounts of carbon dioxide (CO₂)
52 to the atmosphere, which is the main reason for observed global warming. The oceans are a
53 major CO₂ sink accounting for ~25% (~2.5 Pg C yr⁻¹ for the last decade) of the annual

54 anthropogenic CO₂ emissions (Friedlingstein et al., 2020) and ~40% of all anthropogenic CO₂
 55 since industrialization (Gruber et al., 2019; Sabine et al., 2004).



56

57 **Figure 1.** A schematic of the upper ocean (0–10 m depth) using an example where temperature is
 58 influenced by a positive (ocean heat loss) sensible heat flux and CO₂ is being taken up by the ocean.
 59 The grey shaded area represents the thermal boundary layer (TBL), and the red line represents the
 60 temperature gradient in the TBL. The mass (in this case, CO₂) boundary layer (MBL) is embedded
 61 within the TBL. The blue line corresponds to the CO₂ concentration gradient within the MBL. The TBL
 62 is characteristically ten times thicker than the MBL because heat is transferred about an order of
 63 magnitude quicker than CO₂ (Jähne, 2009). $T_{\text{Interface}}$: the temperature at the air-sea interface; T_{Skin} : the
 64 skin temperature at ~10 μm depth measured by an infrared radiometer; T_{Mass} : the temperature at the base
 65 of the MBL (20–200 μm depth); T_{Thermal} : the temperature at the base of the TBL (0.1–2 mm depth);
 66 T_{Subskin} : the temperature of seawater below the TBL at a depth of ~0.1–1 m such as measured by drifting
 67 buoys; T_{Bulk} : the temperature at 1–10 m depth as measured at the typical depth of a ship’s seawater
 68 intake. $T_{\text{Interface}}$, T_{Mass} , and T_{Thermal} are conceptual, whereas T_{Skin} , T_{Subskin} , and T_{Bulk} are from actual
 69 measurements (practical). Sea surface temperature (SST) is a general term for all temperatures
 70 mentioned above. Figure developed from Donlon et al. (2007).

71

72 The global air-sea CO₂ flux is often estimated by the bulk method combining *in-situ* $f\text{CO}_{2w}$
 73 (fugacity of CO₂ in seawater) measurements (e.g., from the Surface Ocean CO₂ Atlas, SOCAT;
 74 Bakker et al., 2016) with a wind speed-dependent gas transfer velocity (e.g., Wanninkhof, 2014;
 75 see Methods). Thanks to the SOCAT (<http://www.socat.info/>) community, a key dataset of

76 $f\text{CO}_{2w}$ has been available since 2011 (Pfeil et al., 2013; Sabine et al., 2013). The latest SOCAT
77 version, SOCAT v2021, contains 30.6 million quality-controlled $f\text{CO}_{2w}$ observations from
78 1957 to 2020 with an accuracy better than 5 μatm (Bakker et al., 2016, 2021).

79 Sea surface temperature (SST) is key for bulk air-sea CO_2 flux estimates. Takahashi et al. (2009)
80 reported a 13% increase in ocean CO_2 uptake by correcting for a 0.08 K warm bias in SST.
81 CO_2 is a water-side controlled gas (Liss & Slater, 1974), and thus air-sea CO_2 exchange is
82 mainly limited by transfer within the $\sim 20\text{--}200\ \mu\text{m}$ mass boundary layer (MBL, Figure 1; Jähne,
83 2009). The MBL temperature should be used for the CO_2 flux calculation, but it is impractical
84 to measure *in-situ* SST within the very thin MBL. The bulk *in-situ* seawater temperature (T_{Bulk})
85 measured concurrently with $f\text{CO}_{2w}$ (typically at $\sim 5\ \text{m}$ depth) in SOCAT is often used for the
86 bulk air-sea CO_2 flux calculation by assuming a well-mixed upper ocean (top $\sim 10\ \text{m}$) without
87 any vertical temperature gradients.

88 However, there are two issues with using the SOCAT SST. Firstly, many processes can
89 generate vertical temperature gradients in the upper ocean. There is a temperature gradient (red
90 line in Figure 1) in the thermal boundary layer (TBL, grey shaded area) relating to air-sea heat
91 exchange. Infrared radiometer measurements indicate that the skin temperature at $\sim 10\ \mu\text{m}$
92 depth (T_{Skin}) is on average $\sim 0.17\ \text{K}$ (Donlon et al., 2002) lower than the subskin temperature
93 (T_{Subskin} , at $\sim 0.1\text{--}1\ \text{m}$ depth) because the ocean surface generally loses heat through longwave
94 radiation, and latent and sensible heat fluxes (the so-called cool skin effect; e.g., Donlon et al.,
95 2007, 2002; Minnett et al., 2011; Robertson & Watson, 1992; Zhang et al., 2020). Another
96 process that might create an upper ocean temperature gradient is the diurnal warm layer effect.
97 Water close to the surface (e.g., at 0.5 m depth) is sometimes warmer than deeper water (e.g.,
98 at 5 m depth) due to daytime solar insolation, especially under conditions of clear sky and low
99 wind speed (Gentemann & Minnett, 2008; Prytherch et al., 2013; Ward et al., 2004). The
100 warming leads to stabilization of the surface layer and thus helps maintain a layered upper
101 ocean structure. The diurnal warm layer effect is not as ubiquitous as the cool skin effect, and
102 the warm layer is complex to characterize. In the absence of the warm layer effect, the bulk
103 seawater temperature (T_{Bulk}) is approximately equal to T_{Subskin} , and T_{Thermal} (temperature at the
104 base of the TBL) because the water below the TBL is well-mixed by turbulence.

105 The second issue is the potential warm bias in the SOCAT SST. The SST community has
106 identified a warm bias in shipboard SST measurements in the ICOADS (International
107 Comprehensive Ocean-Atmosphere Data Set; Huang et al., 2021; Kennedy et al., 2011, 2019;

108 Reynolds & Chelton, 2010). This might be because ship SST measurements are affected by
109 engine room warming (Kennedy et al., 2019). The SSTs in SOCAT were almost exclusively
110 measured by shipboard systems (98%), meaning that a warm bias could also exist in the
111 SOCAT SST dataset.

112 Satellite observation of SST represents a consistent estimate of subskin temperature and avoids
113 the diurnal warm layer effect and any potential warm bias issue. Satellite SST thus has been
114 proposed as an alternative to calculate the bulk air-sea CO₂ flux (Goddijn-Murphy et al., 2015;
115 Shutler et al., 2019; Watson et al., 2020; Woolf et al., 2016). Results, based on a satellite SST
116 dataset suggest a ~25% increase (i.e., warm bias correction; cool skin correction results in
117 another ~25% increase) in ocean CO₂ uptake compared to the flux estimate based on the
118 SOCAT SST (Watson et al., 2020). However, satellite SST is not measured concurrently with
119 the $f\text{CO}_{2w}$. Co-locating the $1^\circ \times 1^\circ$, monthly gridded satellite SSTs with individual $f\text{CO}_{2w}$ in
120 SOCAT might introduce extra uncertainties. In addition, various issues in satellite SSTs (e.g.,
121 cloud masking, impact of aerosol, diurnal variability, uncertainty estimation, and validation)
122 have not been fully resolved, especially at high latitudes and in coastal and highly dynamic
123 regions (O’Carroll et al., 2019). A comparison of eight global gap-free satellite/blended SST
124 products showed that their global mean ranged from 20.02 °C to 20.17 °C for the period
125 2003–2018 (at a 95% confidence level; Yang et al., 2021).

126 SST observations from drifting buoys are unaffected by engine room warming, and are
127 expected to provide the best-quality reference temperature to assess bias in the ship SST, and
128 satellite SST retrievals (Huang et al., 2021; Kennedy et al., 2011, 2019; Kent et al., 2017;
129 Merchant et al., 2019; Reynolds & Chelton, 2010). This work utilizes drifting buoy SST as the
130 reference temperature to determine the accuracy of the SOCAT SST, and to correct for any
131 bias in the SOCAT SST dataset.

132 Subskin temperature with a cool skin correction represents the skin temperature, which can be
133 used to calculate air-sea CO₂ flux. Watson et al. (2020) reported a ~25% increase in ocean CO₂
134 uptake by considering a constant cool skin effect (-0.17 K, Donlon et al., 2002) for 1982 to
135 2020. In this study, the cool skin effect estimated by a physical model (Fairall et al., 1996) and
136 by an empirical model (Donlon et al., 2002) are compared at a global scale. The updated
137 temperature corrections are then used to estimate their impact on the global air-sea CO₂ flux.
138 The revised global air-sea CO₂ flux based on an ensemble of CO₂ flux products (Fay et al.,
139 2021) is then compared with the ocean carbon inventory (Gruber et al., 2019).

140

141 2 Methods

142 2.1 Global Air-Sea CO₂ Flux Estimates

143 The bulk air-sea CO₂ flux equation is:

$$144 \quad F = K_{660}(Sc/660)^{-0.5}(\alpha_w fCO_{2w} - \alpha_i fCO_{2a}) \quad (1)$$

145 where F (mmol m⁻² day⁻¹) is the air-sea CO₂ flux and K_{660} (cm h⁻¹) is the gas transfer velocity
146 (e.g., Wanninkhof, 2014) normalized to a Sc (Schmidt number) of 660. The Sc is defined as
147 the ratio of the kinematic viscosity of water (m² s⁻¹) and the molecular diffusivity of CO₂ (m²
148 s⁻¹). The CO₂ solubility (mol L⁻¹ atm⁻¹) at the base of the MBL and at the air-sea interface are
149 represented by α_w and α_i , respectively (Figure 1). Sc and α are calculated from seawater
150 temperature and salinity (Wanninkhof et al., 2009; Weiss, 1974). Sc is equal to 660 for CO₂ at
151 20 °C and 35 psu seawater. The CO₂ fugacity (μ atm) at the base of the MBL and just above the
152 air-sea interface are represented by fCO_{2w} and fCO_{2a} , respectively.

153 To calculate the global air-sea CO₂ flux, fCO_{2w} measured at the equilibrator temperature is first
154 corrected to the *in-situ* bulk temperature (SOCAT SST). Seawater at ~5 m depth (ranging from
155 1–10 m depth) is sampled from the ship's underway water intake and is pumped through an
156 equilibrator. The equilibrated CO₂ mole fraction in the air of the headspace (χCO_{2w}) is
157 measured in a gas analyzer. χCO_{2w} is then converted to equilibrator fugacity (fCO_{2w_equ}) (Text
158 S1 in Supporting Information S1). fCO_{2w_equ} is further corrected by the chemical temperature
159 normalization (Takahashi et al., 1993) to obtain fCO_{2w} in the bulk seawater:

$$160 \quad fCO_{2w} = fCO_{2w_equ} e^{0.0423(T_{w_bulk} - T_{equ})} \quad (2)$$

161 where T_{w_bulk} is the seawater temperature measured concurrently with fCO_{2w} at the ship's water
162 intake at typically 5 m depth. Seawater fCO_{2w} measurements are then interpolated to obtain a
163 global gap-free fCO_{2w} product (at 1° × 1°, monthly resolution, e.g., Landschützer et al., 2013).
164 A global gap-free SST dataset is generally one of the independent input variables for the fCO_{2w}
165 interpolation process. Other variables in Equation 1 are calculated using a global gap-free SST
166 product and related datasets (e.g., mole fraction of atmospheric CO₂ for the calculation of
167 fCO_{2a}). Finally, globally mapped fCO_{2w} , fCO_{2a} , Sc , α_w , α_i , and gas transfer velocity (K_{660} ,
168 estimated using a global gap-free wind speed dataset) are used for the CO₂ flux calculation via
169 Equation 1.

170
171
172
173
174

Table 1. Variables and relevant sea surface temperature (SST) types for global air-sea CO₂ flux estimates and their relative importance for the flux estimate (after Woolf et al., 2016). The back-of-the-envelope calculation in the last column is for $f\text{CO}_{2w}$ of $\sim 380 \mu\text{atm}$, $f\text{CO}_{2a}$ of $\sim 390 \mu\text{atm}$, and $\Delta f\text{CO}_2$ of $-10 \mu\text{atm}$, values typical for the last decade (Landschützer et al., 2020).

Variable (x)	Conceptual SST	Practical SST product	$\frac{\partial \ln(x)}{\partial T}$	$\frac{\partial \ln(\text{flux})}{\partial T}$
$Sc^{-0.5}$	T_{Bulk}	Global gap-free T_{Subskin}	2.5% K ⁻¹	2.5% K ⁻¹
α_i	$T_{\text{Interface}}$	T_{Skin} (Global gap-free T_{Subskin} with a cool skin correction)	-2.5% K ⁻¹	100% K ⁻¹
$f\text{CO}_{2a}$	$T_{\text{Interface}}$	T_{Skin} (Global gap-free T_{Subskin} with a cool skin correction)	-0.2% K ⁻¹	10% K ⁻¹
α_w	T_{Thermal}	Global gap-free T_{Subskin}	-2.5% K ⁻¹	-100% K ⁻¹
Individual $f\text{CO}_{2w}$	T_{Thermal}	Individual T_{Subskin} (<i>In-situ</i> T_{Bulk} with any bias correction)	4.23% K ⁻¹	160% K ⁻¹
Mapped $f\text{CO}_{2w}$	T_{Thermal}	Global gap-free T_{Subskin}	< 4.23% K ^{-1*}	< 160% K ^{-1*}

175 *The interpolation method (e.g., MPI-SOMFFN neural network technique; Landschützer et al., 2013)
176 can largely dampen the effect of SST on mapped $f\text{CO}_{2w}$.

177
178
179
180
181
182
183
184
185
186
187
188
189
190
191

Table 1 summarizes the SST types that should be used to calculate variables in Equation 1. Sc should be calculated from the temperature utilized to derive K_{660} (e.g., T_{Bulk} for the K_{660} derived from the dual-tracer method; e.g., Ho et al., 2006; Nightingale et al., 2000). The air-sea interface temperature ($T_{\text{Interface}}$) should be used for the calculation of $f\text{CO}_{2a}$ and α_i , while the temperature at the base of the MBL (T_{Mass}) should be employed to calculate $f\text{CO}_{2w}$ (via Equation 2) and α_w . However, Woolf et al. (2016) suggested that T_{Thermal} might be a better temperature for calculating $f\text{CO}_{2w}$ and α_w . The seawater carbonate system creates a unique situation for air-sea CO₂ exchange, which does not exist for other gases. Seawater temperature changes cause chemical repartitioning of the carbonate species (CO₂, carbonic acid, bicarbonate, and carbonate; Zeebe & Wolf-Gladrow, 2001). We find that the timescale of this repartitioning equilibration (e-folding time > 10 s for typical seawater; Johnson, 1982; Zeebe & Wolf-Gladrow, 2001) is much longer than the timescale (~ 1 s) of water mixing below the MBL but within the TBL, where viscous dissipation dominates the water mixing (Jähne, 2009; Jähne et al., 1987; Woolf et al., 2016). The explanation of the timescales is detailed in Text 2

192 in Supporting Information S1. Although there is a temperature gradient in the TBL due to the
193 cool skin effect, the carbonate species are not expected to have time to thermally adjust, which
194 suggests that T_{Thermal} is the optimal temperature for calculating $f\text{CO}_{2\text{w}}$ and α_{w} .

195 T_{Thermal} , T_{Mass} , and $T_{\text{Interface}}$ are conceptual temperatures, which can be approximated by practical
196 temperatures (Figure 1). Satellite SST, which represents the subskin temperature, is a good
197 approximation for T_{Thermal} (Shutler et al., 2019; Watson et al., 2020; Woolf et al., 2016). A
198 satellite T_{Subskin} product can be used to calculate α_{w} and Sc , and to map $f\text{CO}_{2\text{w}}$ for the global
199 ocean. T_{Subskin} with a cool skin correction can then be utilized to calculate global $f\text{CO}_{2\text{a}}$, and α_{i} .
200 *In-situ* T_{Subskin} should ideally be used to correct $f\text{CO}_{2\text{w}}$ from the equilibrator temperature to the
201 subskin seawater temperature. However, the *in-situ* temperature measured concurrently with
202 the $f\text{CO}_{2\text{w}}$ in SOCAT is T_{Bulk} , and *in-situ* T_{Subskin} measurements are unavailable to exactly match
203 the SOCAT space and time-stamp. Using *in-situ* T_{Bulk} (i.e., SOCAT SST) to correct $f\text{CO}_{2\text{w}}$ is
204 reasonable in the absence of a warm layer effect, but it is important to account for the potential
205 warm bias in the SOCAT SST.

206 Table 1 also summarizes the influence of SST and the corresponding importance for the
207 variables used to make air-sea CO_2 flux estimates (after Woolf et al., 2016). The Sc and $f\text{CO}_{2\text{a}}$
208 variations due to the bias in the SST product have a small influence on the global air-sea CO_2
209 flux. However, any bias in the SST data used for the calculation of α_{w} , α_{i} , and especially $f\text{CO}_{2\text{w}}$
210 can result in a considerable bias in the flux. The temperature influence on the $f\text{CO}_{2\text{w}}$ mapping
211 should be significantly dampened by the interpolation process. The most significant influence
212 on the CO_2 flux due to temperature bias comes from individual $f\text{CO}_{2\text{w}}$ ($\sim 160\% \text{ K}^{-1}$, Table 1).
213 An average bias of 0.1 K could result in a bias in $f\text{CO}_{2\text{w}}$ of $\sim 1.6 \mu\text{atm}$, which corresponds to
214 $\sim 16\%$ of the net air-sea CO_2 flux for the last decade (Landschützer et al., 2020).

215 The skin temperature should be used for the calculation of α_{i} and $f\text{CO}_{2\text{a}}$. The T_{Skin} can be
216 obtained from T_{Subskin} with a cool skin correction. If T_{Subskin} is used rather than T_{Skin} for the
217 calculation of α_{i} , and $f\text{CO}_{2\text{a}}$, the ocean CO_2 uptake is in theory underestimated by $\sim 19\%$ for the
218 last decade with a mean cool skin effect of 0.17 K (Donlon et al., 2002).

219

220 **2.2 Bias Assessment**

221 The *in-situ* bulk SST in SOCAT is generally used to correct individual $f\text{CO}_{2\text{w}}$ observations
222 from the equilibrator temperature to the seawater temperature (e.g., studies in Table S1 in

223 Supporting Information S1). However, a warm bias might exist in the SOCAT SST due to
224 heating in the engine room. Watson et al. (2020) co-located the DOISST v2.0 (NOAA Daily
225 Optimum Interpolation SST dataset; Reynolds et al., 2007) with individual *in-situ* SST
226 measurements in SOCAT. They found that the SOCAT SST is on average 0.13 ± 0.78 K higher
227 than the co-located DOISST v2.0. However, Huang et al. (2021) pointed out that there might
228 be a cold bias in the DOISST v2.0 and DOISST v2.1 products (the difference between DOISST
229 v2.0 and v2.1 can be seen in Text S4 in Supporting Information S1) .

230 This study uses accurate SST observed by drifting buoys to assess the potential cold bias in the
231 DOISST v2.1 and the warm bias in SOCAT SST. A drifting buoy SST dataset from iQuam (*in*
232 *situ* SST Quality Monitor v2.10; Xu & Ignatov, 2014) with high accuracy (quality level = 5) is
233 used for the assessment. The buoy SST is first gridded ($1^\circ \times 1^\circ$, monthly) and then compared
234 with the resampled DOISST v2.1 ($1/4^\circ \times 1/4^\circ$, daily data are resampled to $1^\circ \times 1^\circ$, monthly
235 resolution) and the gridded SST ($1^\circ \times 1^\circ$, monthly) in SOCAT v2021.

236

237 **2.3 Cool Skin Effect Estimate**

238 The cool skin effect is ubiquitous in the ocean (Donlon et al., 2002) and should be considered
239 when estimating air-sea CO₂ fluxes. Watson et al. (2020) used a constant value (-0.17 K) to
240 account for the impact of the cool skin effect on air-sea CO₂ fluxes. However, the cool skin
241 effect is affected by many environmental processes. Donlon et al. (2002) proposed a wind
242 speed-dependent cool skin effect based on skin and bulk temperature measurements (Donlon02,
243 hereafter). A physical model for the cool skin effect proposed by Saunders (1967) and
244 developed by Fairall et al. (1996) considers wind speed, longwave radiation, heat flux, and
245 solar radiation (Fairall96, hereafter). Fairall96 has been included in the COARE 3.5 model
246 (Edson et al., 2013) and recent studies (Alappattu et al., 2017; Embury et al., 2012; Zhang et
247 al., 2020) suggest that Fairall96 better accounts for the cool skin effect than the
248 parameterization dependent upon a single variable (wind speed).

249 We employ the ERA5 wind speed data (Hersbach et al., 2020) to estimate the Donlon02 cool
250 skin effect. The COARE 3.5 model is used to estimate the Fairall96 cool skin effect. The
251 following model inputs are used: CCI SST v2.1 (European Space Agency Climate Change
252 Initiative SST product; Merchant et al., 2019; Merchant & Embury, 2020), NCEP sea level
253 pressure (Kalnay et al., 1996), ERA5 monthly averaged reanalysis datasets (Hersbach et al.,

254 2020) for wind speed, 2 m above mean sea level (AMSL) air temperature, relative humidity
255 (calculated from 2 m AMSL air temperature and dewpoint temperature using the August-
256 Roche-Magnus approximation), downward shortwave radiation, downward longwave
257 radiation, and boundary layer height.

258

259 **2.4 Global Air-Sea CO₂ Flux Estimates with the Temperature Correction**

260 We use two different methods to account for the bias in the SOCAT SST for the global air-sea
261 CO₂ flux estimates. For the first method, we use the buoy SST as the reference temperature to
262 assess the bias in SOCAT SST (bias_buoy, hereafter). We correct the 1° × 1°, monthly $f\text{CO}_{2w}$
263 in SOCAT v2021 via Equation 2 (i.e., $f\text{CO}_{2w_corrected} = f\text{CO}_{2w} e^{-0.0423 * \Delta\text{SST}}$) by the temperature
264 difference (ΔSST) between SOCAT SST and buoy SST. The ΔSST varies with latitude (with
265 a 10° latitude running mean, see the orange line in Figure 2b) but does not vary over time. The
266 number of matched data points between SOCAT SST and buoy SST is small in most years, so
267 ΔSST is averaged over 1982 to 2020. In addition, only $f\text{CO}_{2w}$ data within 70°S to 70°N are
268 corrected because of the small number of measurements in the polar oceans. For the second
269 method, the co-located DOISST v2.1 replaces SOCAT SST in Equation 2 to reanalyze $f\text{CO}_{2w}$
270 (bias_OI, hereafter; Watson et al., 2020). The reanalyzed $f\text{CO}_{2w}$ is used for the flux calculation
271 (see Goddijn-Murphy et al., 2015 and Holding et al., 2019 for the reanalysis process).

272 We employ the MPI-SOMFFN neural network technique (Landschützer et al., 2013) to
273 interpolate the $f\text{CO}_{2w_corrected}$ and the reanalyzed $f\text{CO}_{2w}$ to the global ocean from 1982 through
274 2020, using a set of input variables. We use the same datasets as Landschützer et al. (2014) for
275 the neural network inputs, except for the SST product. The CCI SST (Merchant et al., 2019)
276 represents the subskin temperature and is independent of *in-situ* SST measurements, so we
277 utilize the 1° × 1°, monthly CCI SST v2.1 for the neural network training process. The CCI
278 SST v2.1 is also used to calculate Sc and α_w , while the CCI SST v2.1 with a cool skin correction
279 is employed to calculate α_i and $f\text{CO}_{2a}$.

280 We use two models (Fairall96 and Donlon02) to estimate the cool skin effect. Both Fairall96
281 and Donlon02 cool skin effect estimates are applied to the CCI SST v2.1 to calculate α_i and
282 $f\text{CO}_{2a}$, respectively. The quadratic wind speed-dependent formulation ($K_{660} = a U_{10}^2$; Ho et al.,
283 2006; Wanninkhof, 2014) is used to calculate gas transfer velocity. The 1° × 1°, monthly ERA5
284 wind speed data from 1982 to 2020 is utilized to scale the transfer coefficient a to match to a
285 global mean K_{660} of 18.2 cm h⁻¹ from the ¹⁴C inventory method (Naegler, 2009). It is worth

286 noting that the cool skin effect and the warm layer effect do not impact the global mean K_{660}
287 calculated from the ^{14}C inventory because the air-sea ^{14}C concentration difference ($\Delta^{14}\text{C}$) is
288 very large (Naegler, 2009; Sweeney et al., 2007), and the upper ocean temperature gradients
289 only result in a minor change in $\Delta^{14}\text{C}$. In the end, we substitute all variables above into Equation
290 1 to calculate the global air-sea CO_2 flux.

291

292 **3. Results**

293 **3.1 Warm Bias in the *In-situ* SOCAT SST**

294 The temperature assessment using the buoy SST suggests a cold bias in the DOISST v2.1 (0.09
295 K on average) and a small warm bias (0.02 K on average) in the SOCAT SST, which indicates
296 that while a warm bias exists in the SOCAT SST, using the co-located DOISST would
297 overestimate this bias in SOCAT SST (Figure 2a).

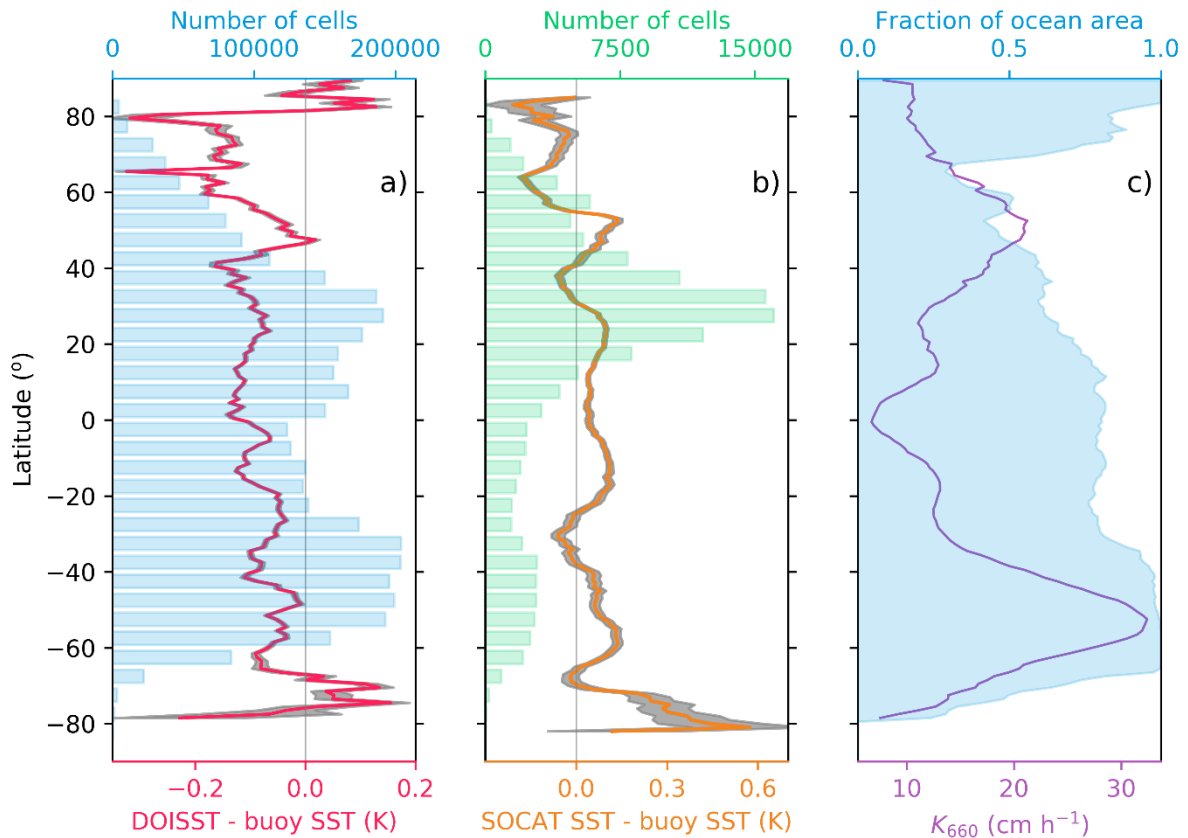
298 Figure 2b shows the latitudinal variation of the bias in SOCAT SST. The number of grid cells
299 with both SOCAT and buoy data (green bars in Figure. 2b) is small and the standard error for
300 the temperature difference (grey shading) is large in the high latitude oceans. Therefore, we
301 only consider data between 70°S and 70°N . The SOCAT SST minus buoy SST (ΔSST , orange
302 line in Figure 2b) shows apparent variation with latitude. ΔSST is on average positive, but is
303 slightly negative at 35°N and 30°S . In the northern hemisphere, ΔSST is $+0.04$ K near the
304 equator and increases by $+0.1$ K to a maximum at 25°N and then decreases to -0.05 K at 35°N .
305 ΔSST also increases from 35°N to a maximum of $+0.15$ K at 50°N and then decreases further
306 north. The ΔSST pattern in the southern hemisphere roughly mirrors that in the northern
307 hemisphere with a 5° northward shift.

308 It is worth noting that under-sampling affects these bias assessments for SOCAT SST. If we
309 consider all paired cells with both buoy and SOCAT SST measurements, the warm bias is on
310 average $+0.02$ K. If we only consider cells with at least ten buoy SST and ten SOCAT SST
311 measurements, the warm bias is on average $+0.03$ K (Figure S2a in Supporting Information
312 S1). The latitudinal variation of the bias is very similar no matter considering how many
313 measurements are within a cell (Figure S2b in Supporting Information S1).

314 It is important to consider latitudinal variation when correcting for bias in SOCAT SST. For
315 instance, SOCAT SST has a relatively large warm bias (thus a large bias in the $f\text{CO}_{2\text{w}}$) in the

316 Southern Ocean (south of 35°S, Figure 2b), which coupled with a high K_{660} and a large surface
 317 ocean area (Figure 2c) results in a substantial bias in Southern Ocean CO₂ flux estimates. This
 318 study uses a latitude-varying temperature bias (i.e., the orange line in Figure 2b) to correct the
 319 air-sea CO₂ flux between 70°S and 70°N (see Section 2.4).

320



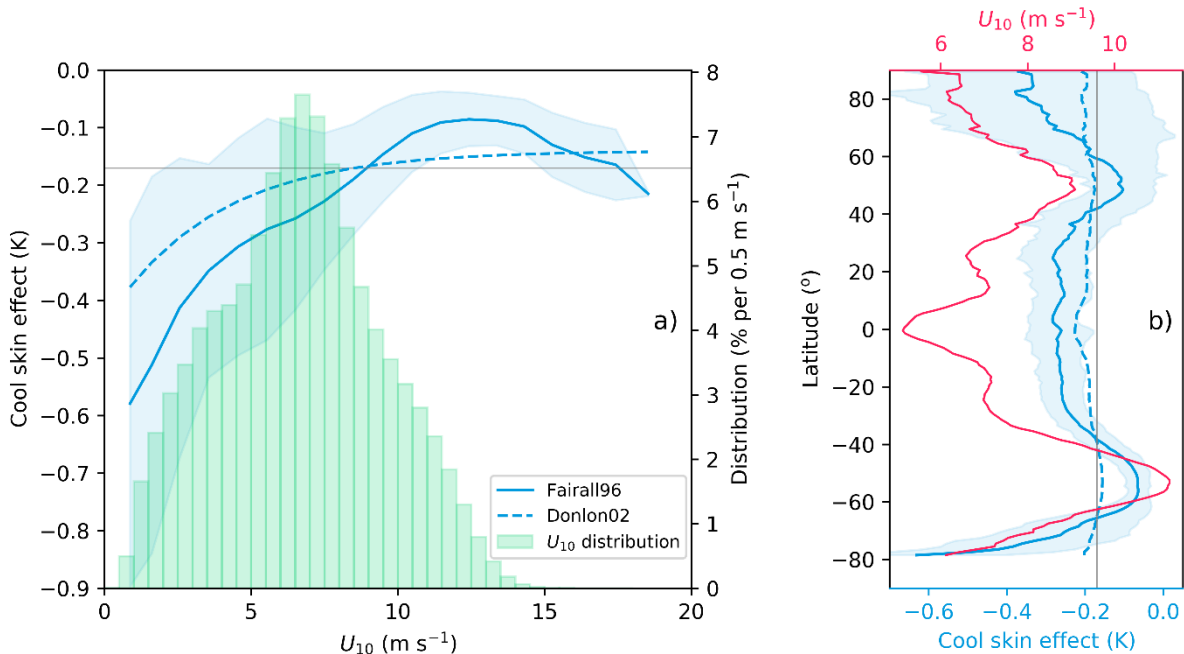
321

322 **Figure 2.** Latitudinal variation in SST differences, number of matched grid cells, the gas transfer
 323 velocity (K_{660}) and the fraction of the globe surface area covered by ocean: (a) 1° latitude average
 324 temperature difference between DOISST v2.1 and buoy SST (red line) \pm 1 standard error (grey shading).
 325 The input data are from 1982 to 2020 and have a 1° \times 1°, monthly resolution, Blue bars show the number
 326 of cells (5° latitude bin) containing both DOISST and buoy SST data; (b) 10° latitude running mean of
 327 the temperature difference between SOCAT SST (from SOCATv2021) and buoy SST (orange line, i.e.,
 328 Δ SST in the main text) \pm 1 standard error (grey shading). Green bars correspond to the number of
 329 cells (5° latitude bin) containing both gridded SOCAT and buoy SST; (c) 1° latitude average K_{660}
 330 (purple line) calculated with a wind speed-dependent parameterization (Ho et al., 2006) using the ERA5
 331 wind speed data (Hersbach et al., 2020) for the global ocean. The blue shaded area corresponds to the
 332 fraction of ocean area in different latitudes (1° latitude average).

333

334 3.2 The Cool Skin Effect

335 Figure 3 shows the cool skin effect estimated by Donlon02 and Fairall96. The Fairall96
 336 estimate of the cool skin effect is stronger than the Donlon02 estimate for low wind speeds
 337 ($U_{10} < 9 \text{ m s}^{-1}$) but weaker for high wind speeds ($9 \text{ m s}^{-1} < U_{10} < 16 \text{ m s}^{-1}$) (Figure 3a). The
 338 monthly wind speed distribution (green bars in Figure 3a) shows that wind speeds less than 9
 339 m s^{-1} account for 80% of the wind conditions. Therefore, the cool skin effect estimated by
 340 Fairall96 is typically stronger than that estimated by Donlon02. The standard deviation of the
 341 Fairall96 cool skin effect is much higher at low wind speeds than at high wind speeds, which
 342 reflects that the drivers (longwave radiation, heat flux, and solar radiation) can produce
 343 substantial variations in the cool skin effect under relatively calm conditions.



344 **Figure 3.** (a) Relationship between the cool skin effect and the 10 m wind speed (U_{10}). Green bars
 345 represent the frequency distribution of the ERA5 monthly averaged reanalysis wind speeds ($1^\circ \times 1^\circ$)
 346 over the global ocean for 1982–2020. (b) Latitudinal variation in U_{10} (red line) and the cool skin effect
 347 (1° latitude bins). Both subplots show the average cool skin effect estimated by the Fairall96 physical
 348 model (Fairall et al., 1996, solid blue line), the Donlon02 wind speed-dependent empirical model
 349 (Donlon et al., 2002, dashed blue line) and a constant value (-0.17 K, grey line; Donlon et al., 2002).
 350 The light blue shaded area in both subplots indicates one standard deviation of the bin averages in
 351 Fairall96 cool skin estimates. Global ocean $1^\circ \times 1^\circ$, monthly datasets are used to estimate the cool skin
 352 effect (see Section 2.3).
 353

354

355 The Donlon02 cool skin effect only has a slight latitudinal variation that is not substantially
356 different from a constant (-0.17 K) value (Figure 3b), which was used by a previous study for
357 air-sea CO₂ flux correction (Watson et al., 2020). In contrast, the Fairall96 cool skin estimate
358 shows a clear latitudinal variation with two relatively small cool skin effect regions at around
359 50°S and 50°N where wind speeds are high. The Fairall96 cool skin effect is stable in the
360 tropical zone and decreases toward both poles to ~50° and then increases at even higher
361 latitudes.

362 In most ocean regions, the Fairall96 cool skin effect follows variations in wind speed.
363 Intriguingly, the Fairall96 cool skin effect is nearly constant within the tropical and subtropical
364 zones, even though the wind speed is much lower near the equator than in the subtropics.
365 Drivers other than wind speed (i.e., latent and sensible heat fluxes, and longwave radiation)
366 might counteract the low wind speed effect in this area.

367

368 **4 Discussion**

369 **4.1 Variation in the CO₂ Flux Correction**

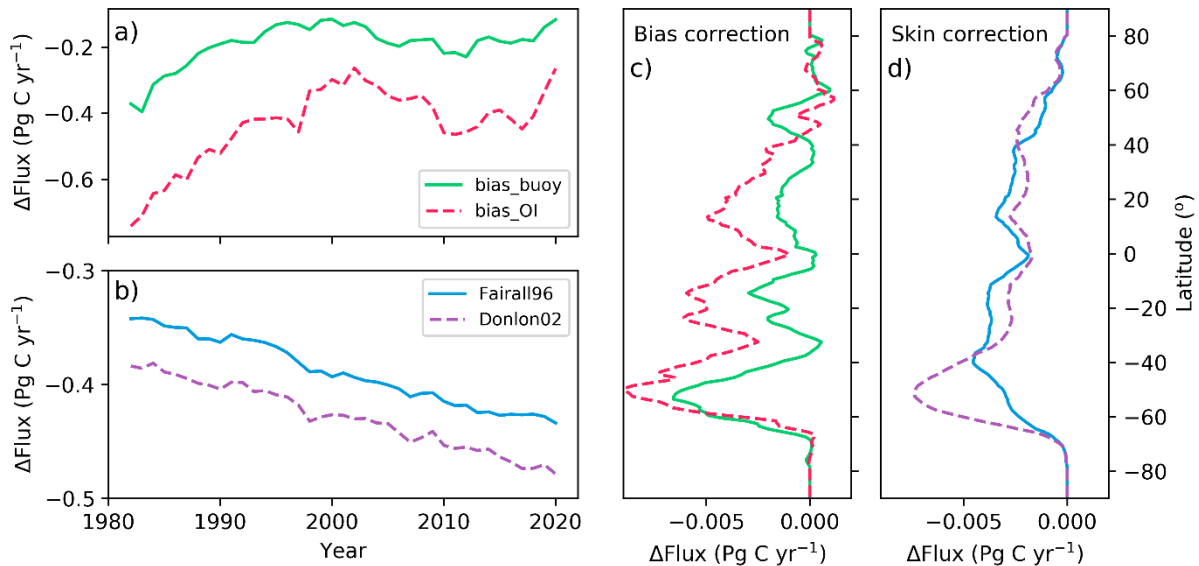
370 In this section, we discuss the impact of the warm bias and cool skin effects on global air-sea
371 CO₂ flux estimates. The corrections are applied over time (between 1982 and 2020, Figure 4a,
372 b) and by latitude (Figure 4c, d).

373 The bias correction using the buoy SST assessment (bias_buoy) leads to an average increase
374 in ocean CO₂ uptake of 0.19 Pg C yr⁻¹, while the bias correction utilizing the co-located
375 DOISST (bias_OI) suggests an average increase of 0.43 Pg C yr⁻¹ (Figure 4a). Adopting the
376 cool skin correction from Fairall96 and Donlon02 increases the 1982–2020 average ocean CO₂
377 uptake by 0.39 Pg C yr⁻¹ and 0.43 Pg C yr⁻¹, respectively (Figure 4b). A constant cool skin
378 correction of -0.17 K increases the flux by an amount similar to using the Donlon02 correction.
379 In total, the flux correction using the bias_buoy and Fairall96 is on average ~0.3 Pg C yr⁻¹
380 lower than if the bias_OI and Donlon02 are used for 1982 to 2020. The inter-annual variation
381 in the net air-sea CO₂ flux with different temperature corrections are shown in Figure S4 in
382 Supporting Information S1.

383 Figure 4a and 4c show the change in the air-sea CO₂ flux (Δ Flux) generated by correcting for
384 the warm bias in SOCAT SST. The temporal and the latitudinal variation of the two flux
385 corrections (bias_buoy and bias_OI) follow similar patterns, but the magnitude is different.

386 Using bias_OI creates a ΔFlux that is twofold larger (in absolute terms) than that using
 387 bias_buoy. The data in Figure 2a suggest that using bias_OI may overestimate the bias in
 388 SOCAT SST, which would result in a $\sim 0.25 \text{ Pg C yr}^{-1}$ overestimation of the air-sea CO_2 flux
 389 correction. Therefore, we favour the bias_buoy correction over the bias_OI correction.

390 While we use the same latitude-varying temperature difference (i.e., bias_buoy) to correct the
 391 bias in SOCAT SST for every year, the flux correction shows clear inter-annual variation
 392 (green line in Figure 4a). One reason is that the number of measurements in each year of SOCAT
 393 is different (Figure S2 in Supporting Information S1), and their spatial distribution differs
 394 between years. The latitude-dependent bias correction, when applied to the different year-to-
 395 year spatial distribution in the SOCAT data, results in a time-varying annual mean bias
 396 correction (Figure S2 in Supporting Information S1).



397

398 **Figure 4.** SST corrections to the air-sea CO_2 flux (ΔFlux) versus time (a, b) and versus latitude (c, d).
 399 SST corrections account for the bias in the SOCAT SST (a, c) and the cool skin effect (b, d). Negative
 400 ΔFlux values represent increased ocean CO_2 uptake. Green and red lines represent ΔFlux due to the bias
 401 correction assessed by drifting buoy SST (bias_buoy) and by co-located DOISST (bias_OI),
 402 respectively. Blue and purple lines represent ΔFlux due to the Fairall96 and the Donlon02 cool skin
 403 corrections, respectively. ΔFlux in a) and b) is the global annual mean, while ΔFlux in (c) and (d) is the
 404 long-term average (1982–2020) in 1° latitude bins. Results are based on the MPI-SOMFFN $f\text{CO}_{2w}$
 405 mapping method (Landschützer et al., 2013) (See Methods). The inter-annual variation of the global
 406 air-sea CO_2 flux with different temperature corrections can be seen in Figure S4 (Supporting
 407 Information S1). Our preferred corrections are bias_buoy for warm bias in SOCAT SST and Fairall96
 408 for the cool skin effect (see Section 4.1).

409

410 Figure 4b and 4d show the change in air-sea CO₂ flux when accounting for the cool skin effect
411 using the Fairall96 and Donlon02 models. Figure 4b indicates an increase over time in both
412 flux corrections (absolute value), which is driven by the increase in $f\text{CO}_{2a}$ (see equation 1 and
413 table 1). The impact of the cool skin effect on the air-sea CO₂ flux is through $\alpha_i * f\text{CO}_{2a}$. The
414 ever-rising atmospheric CO₂ concentration and thus $f\text{CO}_{2a}$, result in the growing cool skin flux
415 correction.

416 The flux correction using Donlon02 exceeds that by Fairall96 by $\sim 0.05 \text{ Pg C yr}^{-1}$ (in absolute
417 terms). The largest difference in flux between the two cool skin corrections occurs in the
418 Southern Ocean (Figure 4d). The Donlon02 cool skin effect has minimal latitudinal variation,
419 so the flux correction is largest at $\sim 50^\circ\text{S}$ where the gas transfer velocity is maximum and the
420 ocean area is relatively large (Figure 2c). The Fairall96 cool skin effect has an apparent
421 latitudinal variation and a minimum (absolute) value at $\sim 50^\circ\text{S}$. This minimum cool skin effect
422 offsets the maximum wind speed and large ocean area, resulting in a smaller flux correction
423 (in absolute terms) at $\sim 50^\circ\text{S}$ for Fairall96 than for Donlon02. Recent work (Alappattu et al.,
424 2017; Embury et al., 2012; Zhang et al., 2020) has suggested that the Fairall96 cool skin model
425 is better than Donlon02 at capturing the cool skin effect at a global scale and this, coupled with
426 our estimates indicates that using the Donlon02 model may lead to an over-correction of the
427 air-sea CO₂ flux, especially in the Southern Ocean.

428

429 **4.2 Implications for Air-Sea CO₂ Flux Estimates**

430 This study deals with the potential bias in the $f\text{CO}_{2w}$ -based air-sea CO₂ flux estimates due to
431 upper ocean temperature effects. A large amount of uncertainty in this $f\text{CO}_{2w}$ -based flux also
432 comes from the gas transfer velocity (Woolf et al., 2019). The air-sea CO₂ flux estimated from
433 the ocean carbon inventory (Gruber et al., 2019) does not require the gas transfer velocity, is
434 unaffected by upper ocean temperature effects and provides an independent estimate of ocean
435 CO₂ uptake. To compare the $f\text{CO}_{2w}$ -based net air-sea CO₂ flux with the anthropogenic air-sea
436 CO₂ flux of the ocean carbon inventory, we need to adjust for river-induced CO₂ outgassing.
437 The riverine carbon flux has been estimated as $0.23 \text{ Pg C yr}^{-1}$ (Lacroix et al., 2020), 0.45 Pg C
438 yr^{-1} (Jacobson et al., 2007), and $0.78 \text{ Pg C yr}^{-1}$ (Resplandy et al., 2018). Here we adopt the
439 mean of these values ($0.49 \pm 0.28 \text{ Pg C yr}^{-1}$).

440 The net air-sea CO₂ flux derived from the ocean carbon inventory for 1994 to 2007 is $-2.1 \pm$
 441 0.4 Pg C yr^{-1} (i.e., $-2.6 \text{ Pg C yr}^{-1}$ anthropogenic flux plus $0.49 \text{ Pg C yr}^{-1}$ river carbon flux; see
 442 the footnote of Table 2 for the propagated uncertainty) (Gruber et al., 2019), which is shown
 443 in Table 2 along with the ensemble mean of eighteen $f\text{CO}_{2w}$ -based fluxes (Fay et al., 2021).
 444 Fluxes from six $f\text{CO}_{2w}$ products and three wind speed products (three wind products are used
 445 for each $f\text{CO}_{2w}$ product) are utilized to generate the ensemble mean flux, where missing $f\text{CO}_{2w}$
 446 has been filled with a scaled climatology and gas transfer velocity (K_{660}) has been calibrated to
 447 a global average of 18.2 cm hr^{-1} over the ice-free ocean based on ¹⁴C-bomb flux estimates (Fay
 448 et al., 2021). All six $f\text{CO}_{2w}$ products (which include the MPI SOMFFN method) have been
 449 developed from the SOCAT v2021 dataset. So the corrections of the ensemble mean flux for
 450 the temperature effects should be similar to the corrections in this study based on the MPI-
 451 SOMFFN $f\text{CO}_{2w}$ mapping method (Landschützer et al., 2013). Furthermore, an ensemble of
 452 different data interpolation methods and different wind products provides a more robust flux
 453 estimate than a single interpolation method based on a single wind product. The flux
 454 corrections estimated in this study are applied to the ensemble mean flux.

455

456 **Table 2.** Global mean net air-sea CO₂ fluxes for 1994 to 2007. Here bias_buoy and bias_OI represent
 457 the bias correction (to SOCAT SST) using the assessment from buoy SST and co-located DOISST,
 458 respectively. Fairall96 (Fairall et al., 1996) and Donlon02 (Donlon et al., 2002) correspond to the cool
 459 skin effect estimated by the physical and the empirical model, respectively. We favour the bias_buoy
 460 and Fairall96 corrections (see Section 4.1)

Net air-sea CO ₂ flux estimates (Pg C yr ⁻¹)	Flux without a temperature correction	Flux with warm bias correction		Flux with warm bias and cool skin correction	
		bias_buoy	bias_OI	bias_buoy + Fairall96	bias_OI + Donlon02
Ensemble mean of $f\text{CO}_{2w}$ -based fluxes*	-1.7 ± 0.4	-1.8 ± 0.4	-2.0 ± 0.4	-2.2 ± 0.4	-2.4 ± 0.4
Ocean carbon inventory**	-2.1 ± 0.4				

461 *The ensemble mean of the fluxes from six $f\text{CO}_2$ products and three wind speed products (Fay et al.,
 462 2021).

463 **From Gruber et al. (2019) ($-2.6 \pm 0.3 \text{ Pg C yr}^{-1}$) with a riverine-derived carbon flux adjustment (0.49
 464 $\pm 0.28 \text{ Pg C yr}^{-1}$). The uncertainty (i.e., $\pm 0.4 \text{ Pg C yr}^{-1}$) is calculated as $\sqrt{0.3^2 + 0.28^2} \text{ Pg C yr}^{-1}$.

465

466 The ensemble mean air-sea CO₂ flux without any bias and cool skin corrections (-1.7 ± 0.4 Pg
467 C yr⁻¹) is barely within the combined uncertainty of the net flux estimate from the ocean carbon
468 inventory. The ensemble mean CO₂ flux with bias_buoy and Fairall96 cool skin corrections is
469 -2.2 ± 0.4 Pg C yr⁻¹, similar to the ocean carbon inventory derived net ocean CO₂ uptake. The
470 corrections using the bias_OI and the Donlon02 suggested by a previous study (Watson et al.,
471 2020) pushes the ensemble mean air-sea CO₂ flux (-2.4 ± 0.4 Pg C yr⁻¹) towards the lower
472 limit of the ocean carbon inventory flux estimate (Table 2).

473 Another question is whether the warm bias and cool skin flux corrections conflict with our
474 understanding of air-sea CO₂ fluxes. One might argue that the preindustrial ocean and
475 atmosphere would have been in a natural equilibrium (i.e., the global total of steady state of
476 natural air-sea CO₂ fluxes would have been zero; see Hauck et al., 2020 for details), but the
477 temperature corrections would create a preindustrial ocean carbon sink. However, the warm
478 bias in SOCAT SST is not a natural phenomenon and should not affect the preindustrial flux
479 estimate. Furthermore, while the cool skin is a natural phenomenon, the flux correction due to
480 the cool skin effect includes both natural and anthropogenic contributions. Figure 4b shows
481 that the cool skin flux correction decreased almost linearly by ~ 0.1 Pg C yr⁻¹ (from -0.34 to $-$
482 0.43 Pg C yr⁻¹) due to the increase in atmospheric CO₂ (~ 70 ppm or $\mu\text{mol mol}^{-1}$, from 341 to
483 414 ppm) from 1982 to 2020 (Dlugokencky & Tans, 2018). Preindustrial atmospheric CO₂ was
484 ~ 260 – 280 ppm (Wigley, 1983), which is ~ 70 ppm lower than atmospheric CO₂ in 1982. Thus,
485 the preindustrial natural air-sea CO₂ flux correction due to the cool skin effect could be ~ -0.25
486 Pg C yr⁻¹, with the remaining correction (~ -0.2 Pg C yr⁻¹ in 2020) due to the increase in
487 atmospheric CO₂ by anthropogenic emissions.

488 A flux correction for the cool skin effect is only related to the $f\text{CO}_{2w}$ observation-based flux
489 estimate, which is available from the 1980s onwards (Friedlingstein et al., 2020). There were
490 no $f\text{CO}_{2w}$ measurements in preindustrial times, so the total preindustrial air-sea CO₂ flux (the
491 sum of steady state natural flux and river flux) is based on model studies, theory, and lateral
492 transport constraints (Hauck et al., 2020). Although the cool skin effect might result in an \sim
493 0.25 Pg C yr⁻¹ flux, we can still assume that ocean and atmosphere were in a natural equilibrium
494 in preindustrial times. Specifically, the cool skin effect has been implicitly included in the
495 preindustrial natural equilibrium assumption. Therefore, this study improves our understanding
496 by suggesting a stronger anthropogenic contribution to the air-sea CO₂ flux, while there is no
497 contradiction between the temperature correction and the preindustrial natural equilibrium
498 assumption.

499 The cool skin effect and its impact on the air-sea CO₂ flux have been discussed for decades.
500 While the cool skin effect itself has been well observed and modelled, its impact on the air-sea
501 CO₂ flux is mainly based on theoretical arguments. We still lack strong observational evidence
502 to confirm the need to include the cool skin effect on estimates of air-sea CO₂ flux – an
503 important topic we urge the community to demonstrate experimentally. The eddy covariance
504 method (e.g., Dong et al., 2021) provides direct flux measurements, that could be used as a
505 reference CO₂ flux to assess the accuracy of the bulk CO₂ flux. Long-term eddy covariance
506 measurements at a place with very low $\Delta f\text{CO}_2$ would be insightful because the relative effect
507 of cool skin on the bulk CO₂ flux is in theory more prominent for regions of low $\Delta f\text{CO}_2$.
508 Appropriate laboratory experiments may yield further insight.

509 In summary, this work updates the temperature corrections to $f\text{CO}_{2w}$ -based air-sea CO₂ flux
510 estimates. It shows that there is a slight warm bias in SOCAT SST and a latitude-varying cool
511 skin effect, resulting in $\sim 0.6 \text{ Pg C yr}^{-1}$ additional ocean CO₂ uptake for 1982 to 2020. The
512 corrected air-sea CO₂ flux for an ensemble of six gap filled air-sea CO₂ flux products agrees
513 well with the ocean carbon inventory derived net flux. The extreme sensitivity of $f\text{CO}_{2w}$ and
514 thus of the air-sea CO₂ flux to the accuracy of SST means that we should be carefully choose
515 the reference temperature to assess any bias in the SOCAT SST. The importance of the
516 Southern Ocean for atmospheric CO₂ uptake, and the strong winds encountered there mean that
517 large scale assessments need a suitable model for the cool skin correction to the air-sea CO₂
518 flux.

519

520

521 **Acknowledgements**

522 We are grateful to H. Zhang (NOAA), C. Merchant (University of Reading), and H. Beggs (Bureau of
523 Meteorology, Australia) for their advice on choosing the appropriate SST product, as well as to J.
524 Kennedy (Met Office Hadley Centre), and S. Zhou (British Antarctic Survey) for suggestions on
525 assessing the bias in the SOCAT SST. We also greatly appreciate the inspirational and helpful
526 discussions with R. Wanninkhof (NOAA) and J. Shutler (University of Exeter). The Surface Ocean
527 CO₂ Atlas (SOCAT) is an international effort, endorsed by the International Ocean Carbon
528 Coordination Project (IOCCP), the Surface Ocean Lower Atmosphere Study (SOLAS) and the
529 Integrated Marine Biogeochemistry and Ecosystem Research program (IMBER), to deliver a uniformly
530 quality-controlled surface ocean CO₂ database. The many researchers and funding agencies responsible
531 for the collection of data and quality control are thanked for their contributions to SOCAT. In this study,

532 Y. Dong has been supported by the China Scholarship Council (CSC/201906330072). The Natural
533 Environment Research Council (NERC) has enabled D. C. E. Bakker's work (PICCOLO,
534 NE/P021395/1, and CUSTARD, NE/P021263/1 projects). The contributions of T.G. Bell and M. Yang
535 have been made possible by support from the NERC (ORCHESTRA, NE/N018095/1, and PICCOLO
536 NE/P021409/1 projects) and European Space Agency AMT4oceanSatFluxCCN
537 (4000125730/18/NL/FF/gp).

538

539 **Open Research**

540 Data can be accessed as follows. Gridded SOCAT v2021 data: [https://www.socat.info/index.php/data-](https://www.socat.info/index.php/data-access/)
541 [access/](https://www.socat.info/index.php/data-access/). Reanalyzed sea surface CO₂ fugacity dataset using co-located DOISST: [https://doi.org/10.181](https://doi.org/10.18160/vmt4-4563)
542 [60/vmt4-4563](https://doi.org/10.18160/vmt4-4563). *In-situ* SST measurements (including the drifting buoy SST and the ship SST): [https://](https://www.star.nesdis.noaa.gov/socd/sst/iquam/data.html)
543 www.star.nesdis.noaa.gov/socd/sst/iquam/data.html. CCI SST v2.1: [https://surftemp.net/regridding/in](https://surftemp.net/regridding/index.html)
544 [dex.html](https://surftemp.net/regridding/index.html). DOISST v2.1: [https://www.ncei.noaa.gov/data/sea-surface-temperature-optimum-interpolati](https://www.ncei.noaa.gov/data/sea-surface-temperature-optimum-interpolated-on/v2.1/access/avhrr/)
545 [on/v2.1/access/avhrr/](https://www.ncei.noaa.gov/data/sea-surface-temperature-optimum-interpolated-on/v2.1/access/avhrr/). ECMWF monthly averaged reanalysis data: [https://cds.climate.copernicus.eu/c](https://cds.climate.copernicus.eu/cdsapp#!/dataset/reanalysis-era5-single-levels-monthly-means?tab=form)
546 [dsapp#!/dataset/reanalysis-era5-single-levels-monthly-means?tab=form](https://cds.climate.copernicus.eu/cdsapp#!/dataset/reanalysis-era5-single-levels-monthly-means?tab=form).

547

548

549 **References**

550 Alappattu, D. P., Wang, Q., Yamaguchi, R., Lind, R. J., Reynolds, M., & Christman, A. J. (2017). Warm
551 layer and cool skin corrections for bulk water temperature measurements for air-sea interaction
552 studies. *Journal of Geophysical Research: Oceans*, 122(8), 6470–6481.
553 <https://doi.org/10.1002/2017JC012688>

554 Bakker, D. C. E., Alin, S., Castaño-Primo, R., Cronin, M., Gkrizalis, T., Kozyr, A., et al. (2021).
555 SOCAT version 2021 for quantification of ocean CO₂ uptake. Available at
556 <https://www.socat.info/index.php/data-access/>. Released 15 June 2021.

557 Bakker, D. C. E., Pfeil, B., Landa, C. S., Metzl, N., O'Brien, K. M., Olsen, A., et al. (2016). A multi-
558 decade record of high-quality *f*CO₂ data in version 3 of the Surface Ocean CO₂ Atlas (SOCAT).
559 *Earth System Science Data*, 8(2), 383–413. <https://doi.org/10.5194/essd-8-383-2016>

560 Dlugokencky, E., & Tans, P. (2018). Trends in atmospheric carbon dioxide, National Oceanic &
561 Atmospheric Administration, Earth System Research Laboratory (NOAA/ESRL). Available at
562 <https://www.socat.info/index.php/data-access/>. Last access: 4 February 2022.

563 Dong, Y., Yang, M., Bakker, D. C. E., Kitidis, V., & Bell, T. G. (2021). Uncertainties in eddy

564 covariance air–sea CO₂ flux measurements and implications for gas transfer velocity
565 parameterisations. *Atmospheric Chemistry and Physics*, 21(10), 8089–8110.
566 <https://doi.org/10.5194/acp-21-8089-2021>

567 Donlon, C. J., Robinson, I., Casey, K. S., Vazquez-Cuervo, J., Armstrong, E., Arino, O., et al. (2007).
568 The global ocean data assimilation experiment high-resolution sea surface temperature pilot
569 project. *Bulletin of the American Meteorological Society*, 88(8), 1197–1214.
570 <https://doi.org/10.1175/BAMS-88-8-1197>

571 Donlon, C. J., Minnett, P. J., Gentemann, C., Nightingale, T. J., Barton, I. J., Ward, B., & Murray, M.
572 J. (2002). Toward improved validation of satellite sea surface skin temperature measurements for
573 climate research. *Journal of Climate*, 15(4), 353–369. [https://doi.org/10.1175/1520-0442\(2002\)015<0353:TIVOSS>2.0.CO;2](https://doi.org/10.1175/1520-0442(2002)015<0353:TIVOSS>2.0.CO;2)

575 Edson, J. B., Jampana, V., Weller, R. A., Bigorre, S. P., Plueddemann, A. J., Fairall, C. W., et al. (2013).
576 On the exchange of momentum over the open ocean. *Journal of Physical Oceanography*, 43(8),
577 1589–1610. <https://doi.org/10.1175/JPO-D-12-0173.1>

578 Embury, O., Merchant, C. J., & Corlett, G. K. (2012). A reprocessing for climate of sea surface
579 temperature from the along-track scanning radiometers: Initial validation, accounting for skin and
580 diurnal variability effects. *Remote Sensing of Environment*, 116, 62–78.
581 <https://doi.org/10.1016/j.rse.2011.02.028>

582 Fairall, C. W., Bradley, E. F., Godfrey, J. S., Wick, G. A., Edson, J. B., & Young, G. S. (1996). Cool-
583 skin and warm-layer effects on sea surface temperature. *Journal of Geophysical Research: Oceans*,
584 101(C1), 1295–1308. <https://doi.org/10.1029/95JC03190>

585 Fay, A. R., Gregor, L., Landschützer, P., McKinley, G. A., Gruber, N., Gehlen, M., et al. (2021).
586 SeaFlux: Harmonization of air-sea CO₂ fluxes from surface pCO₂ data products using a
587 standardized approach. *Earth System Science Data*, 13(10), 4693–4710.
588 <https://doi.org/10.5194/essd-13-4693-2021>

589 Friedlingstein, P., O’Sullivan, M., Jones, M. W., Andrew, R. M., Hauck, J., Olsen, A., et al. (2020).
590 Global carbon budget 2020. *Earth System Science Data*, 12(4), 3269–3340.
591 <https://doi.org/10.5194/essd-12-3269-2020>

592 Gentemann, C. L., & Minnett, P. J. (2008). Radiometric measurements of ocean surface thermal
593 variability. *Journal of Geophysical Research: Oceans*, 113(C8).
594 <https://doi.org/10.1029/2007JC004540>

595 Goddijn-Murphy, L. M., Woolf, D. K., Land, P. E., Shutler, J. D., & Donlon, C. (2015). The OceanFlux
596 Greenhouse Gases methodology for deriving a sea surface climatology of CO₂ fugacity in support

597 of air-sea gas flux studies. *Ocean Science*, 11(4), 519–541. <https://doi.org/10.5194/os-11-519->
598 [2015](https://doi.org/10.5194/os-11-519-2015)

599 Gruber, N., Clement, D., Carter, B. R., Feely, R. A., van Heuven, S., Hoppema, M., et al. (2019). The
600 oceanic sink for anthropogenic CO₂ from 1994 to 2007. *Science*, 363(6432), 1193–1199.
601 <https://doi.org/10.1126/science.aau5153>

602 Hauck, J., Zeising, M., Le Quéré, C., Gruber, N., Bakker, D. C. E., Bopp, L., et al. (2020). Consistency
603 and challenges in the ocean carbon sink estimate for the global carbon budget. *Frontiers in Marine*
604 *Science*, 7(October), 1–22. <https://doi.org/10.3389/fmars.2020.571720>

605 Hersbach, H., Bell, B., Berrisford, P., Hirahara, S., Horányi, A., Muñoz-Sabater, J., et al. (2020). The
606 ERA5 global reanalysis. *Quarterly Journal of the Royal Meteorological Society*, 146(730), 1999–
607 2049. <https://doi.org/10.1002/qj.3803>

608 Ho, D. T., Law, C. S., Smith, M. J., Schlosser, P., Harvey, M., & Hill, P. (2006). Measurements of air-
609 sea gas exchange at high wind speeds in the Southern Ocean: Implications for global
610 parameterizations. *Geophysical Research Letters*, 33(16). <https://doi.org/10.1029/2006GL026817>

611 Holding, T., Ashton, I. G., Shutler, J. D., Land, P. E., Nightingale, P. D., Rees, A. P., et al. (2019). The
612 fluxengine air-sea gas flux toolbox: Simplified interface and extensions for in situ analyses and
613 multiple sparingly soluble gases. *Ocean Science*, 15(6), 1707–1728. <https://doi.org/10.5194/os->
614 [15-1707-2019](https://doi.org/10.5194/os-15-1707-2019)

615 Huang, B., Liu, C., Banzon, V., Freeman, E., Graham, G., Hankins, B., et al. (2021). Improvements of
616 the daily optimum interpolation sea surface temperature (DOISST) version 2.1. *Journal of Climate*,
617 34(8), 2923–2939. <https://doi.org/10.1175/JCLI-D-20-0166.1>

618 Jacobson, A. R., Mikaloff Fletcher, S. E., Gruber, N., Sarmiento, J. L., & Gloor, M. (2007). A joint
619 atmosphere-ocean inversion for surface fluxes of carbon dioxide: 1. Methods and global-scale
620 fluxes. *Global Biogeochemical Cycles*, 21, GB1019. <https://doi.org/10.1029/2005GB002556>

621 Jähne, B. (2009). Air-sea gas exchange. *Elements of Physical Oceanography: A Derivative of the*
622 *Encyclopedia of Ocean Sciences*, 160–169. <https://doi.org/10.1016/B978-0-12-409548-9.11613->
623 [6](https://doi.org/10.1016/B978-0-12-409548-9.11613-6)

624 Jähne, B., Heinz, G., & Dietrich, W. (1987). Measurement of the diffusion coefficients of sparingly
625 soluble gases in water. *Journal of Geophysical Research: Oceans*, 92(C10), 10767–10776.
626 <https://doi.org/10.1029/JC092iC10p10767>

627 Johnson, K. S. (1982). Carbon dioxide hydration and dehydration kinetics in seawater. *Limnology and*
628 *Oceanography*, 27(5), 849–855. <https://doi.org/10.4319/lo.1982.27.5.0849>

- 629 Kalnay, E., Kanamitsu, M., Kistler, R., Collins, W., Deaven, D., Gandin, L., et al. (1996). The
630 NCEP/NCAR 40-year reanalysis project. *Bulletin of the American Meteorological Society*, 77(3),
631 437–472. [https://doi.org/10.1175/1520-0477\(1996\)077<0437:TNYRP>2.0.CO;2](https://doi.org/10.1175/1520-0477(1996)077<0437:TNYRP>2.0.CO;2)
- 632 Kennedy, J. J., Rayner, N. A., Smith, R. O., Parker, D. E., & Saunby, M. (2011). Reassessing biases
633 and other uncertainties in sea surface temperature observations measured in situ since 1850: 2.
634 Biases and homogenization. *Journal of Geophysical Research*, 116(D14), 1–22.
635 <https://doi.org/10.1029/2010jd015220>
- 636 Kennedy, J. J., Rayner, N. A., Atkinson, C. P., & Killick, R. E. (2019). An ensemble data set of sea
637 surface temperature change from 1850: The Met Office Hadley Centre HadSST.4.0.0.0 data set.
638 *Journal of Geophysical Research: Atmospheres*, 124(14), 7719–7763.
639 <https://doi.org/10.1029/2018JD029867>
- 640 Kent, E. C., Kennedy, J. J., Smith, T. M., Hirahara, S., Huang, B., Kaplan, A., et al. (2017). A call for
641 new approaches to quantifying biases in observations of sea surface temperature. *Bulletin of the*
642 *American Meteorological Society*, 98(8), 1601–1616. [https://doi.org/10.1175/BAMS-D-15-](https://doi.org/10.1175/BAMS-D-15-00251.1)
643 [00251.1](https://doi.org/10.1175/BAMS-D-15-00251.1)
- 644 Lacroix, F., Ilyina, T., & Hartmann, J. (2020). Oceanic CO₂ outgassing and biological production
645 hotspots induced by pre-industrial river loads of nutrients and carbon in a global modeling
646 approach. *Biogeosciences*, 17(1), 55–88. <https://doi.org/10.5194/bg-17-55-2020>
- 647 Landschützer, P., Gruber, N., Bakker, D. C. E., Schuster, U., Nakaoka, S., Payne, M. R., et al. (2013).
648 A neural network-based estimate of the seasonal to inter-annual variability of the Atlantic Ocean
649 carbon sink. *Biogeosciences*, 10(11), 7793–7815. <https://doi.org/10.5194/bg-10-7793-2013>
- 650 Landschützer, P., Gruber, N., & Bakker, D. C. E. (2020). An observation-based global monthly gridded
651 sea surface pCO₂ and air-sea CO₂ flux product from 1982 onward and its monthly climatology.
652 *NCEI Accession*, 160558.
- 653 Landschützer, P., Gruber, N., Bakker, D. C. E., & Schuster, U. (2014). Recent variability of the global
654 ocean carbon sink. *Global Biogeochemical Cycles*, 28(9), 927–949.
655 <https://doi.org/10.1002/2014GB004853>
- 656 Liss, P. S., & Slater, P. G. (1974). Flux of gases across the air-sea interface. *Nature*, 247(5438), 181–
657 184. <https://doi.org/10.1038/247181a0>
- 658 Merchant, C. J., & Embury, O. (2020). Adjusting for desert-dust-related biases in a climate data record
659 of sea surface temperature. *Remote Sensing*, 12(16), 1–15. <https://doi.org/10.3390/RS12162554>
- 660 Merchant, C. J., Embury, O., Bulgin, C. E., Block, T., Corlett, G. K., Fiedler, E., et al. (2019). Satellite-

661 based time-series of sea-surface temperature since 1981 for climate applications. *Scientific Data*,
662 6(1), 1–18. <https://doi.org/10.1038/s41597-019-0236-x>

663 Minnett, P. J., Smith, M., & Ward, B. (2011). Measurements of the oceanic thermal skin effect. *Deep-*
664 *Sea Research Part II: Topical Studies in Oceanography*, 58(6), 861–868.
665 <https://doi.org/10.1016/j.dsr2.2010.10.024>

666 Naegler, T. (2009). Reconciliation of excess ¹⁴C-constrained global CO₂ piston velocity estimates.
667 *Tellus, Series B: Chemical and Physical Meteorology*, 61 (2), 372–384.
668 <https://doi.org/10.1111/j.1600-0889.2008.00408.x>

669 Nightingale, P. D., Malin, G., Law, C. S., Watson, A. J., Liss, P. S., Liddicoat, M. I., et al. (2000). In
670 situ evaluation of air-sea gas exchange parameterizations using novel conservative and volatile
671 tracers. *Global Biogeochemical Cycles*, 14(1), 373–387. <https://doi.org/10.1029/1999GB900091>

672 O’Carroll, A. G., Armstrong, E. M., Beggs, H., Bouali, M., Casey, K. S., Corlett, G. K., et al. (2019).
673 Observational needs of sea surface temperature. *Frontiers in Marine Science*, 7:571720.
674 <https://doi.org/10.3389/fmars.2019.00420>

675 Pfeil, B., Olsen, A., Bakker, D. C. E., Hankin, S., Koyuk, H., Kozyr, A., et al. (2013). A uniform, quality
676 controlled Surface Ocean CO₂ Atlas (SOCAT). *Earth System Science Data*, 5(1), 125–143.
677 <https://doi.org/10.5194/essd-5-125-2013>

678 Prytherch, J., Farrar, J. T., & Weller, R. A. (2013). Moored surface buoy observations of the diurnal
679 warm layer. *Journal of Geophysical Research: Oceans*, 118(9), 4553–4569.
680 <https://doi.org/10.1002/jgrc.20360>

681 Resplandy, L., Keeling, R. F., Rödenbeck, C., Stephens, B. B., Khatiwala, S., Rodgers, K. B., et al.
682 (2018). Revision of global carbon fluxes based on a reassessment of oceanic and riverine carbon
683 transport. *Nature Geoscience*, 11(7), 504–509. <https://doi.org/10.1038/s41561-018-0151-3>

684 Reynolds, R. W., & Chelton, D. B. (2010). Comparisons of daily sea surface temperature analyses for
685 2007-08. *Journal of Climate*, 23(13), 3545–3562. <https://doi.org/10.1175/2010JCLI3294.1>

686 Reynolds, R. W., Smith, T. M., Liu, C., Chelton, D. B., Casey, K. S., & Schlax, M. G. (2007). Daily
687 high-resolution-blended analyses for sea surface temperature. *Journal of Climate*, 20(22), 5473–
688 5496. <https://doi.org/10.1175/2007JCLI1824.1>

689 Robertson, J. E., & Watson, A. J. (1992). Thermal skin effect of the surface ocean and its implications
690 for CO₂ uptake. *Nature*, 358(6389), 738–740. <https://doi.org/10.1038/358738a0>

691 Sabine, C. L., Feely, R. A., Gruber, N., Key, R. M., Lee, K., Bullister, J. L., et al. (2004). The oceanic
692 sink for anthropogenic CO₂. *Science*, 305(5682), 367–371.

- 693 <https://doi.org/10.1126/science.1097403>
- 694 Sabine, C. L., Hankin, S., Koyuk, H., Bakker, D. C. E., Pfeil, B., Olsen, A., et al. (2013). Surface Ocean
695 CO₂ Atlas (SOCAT) gridded data products. *Earth System Science Data*, 5(1), 145–153.
696 <https://doi.org/10.5194/essd-5-145-2013>
- 697 Saunders, P. M. (1967). The temperature at the ocean-air interface. *Journal of Atmospheric Sciences*,
698 24(3), 269–273. [https://doi.org/10.1175/1520-0469\(1967\)024<0269:TTATOA>2.0.CO;2](https://doi.org/10.1175/1520-0469(1967)024<0269:TTATOA>2.0.CO;2)
- 699 Shutler, J. D., Wanninkhof, R., Nightingale, P. D., Woolf, D. K., Bakker, D. C. E., Watson, A., et al.
700 (2019). Satellites will address critical science priorities for quantifying ocean carbon. *Frontiers in*
701 *Ecology and the Environment*, 18(1): 27– 35. <https://doi.org/10.1002/fee.2129>
- 702 Sweeney, C., Gloor, E., Jacobson, A. R., Key, R. M., McKinley, G., Sarmiento, J. L., & Wanninkhof,
703 R. (2007). Constraining global air-sea gas exchange for CO₂ with recent bomb ¹⁴C measurements.
704 *Global Biogeochemical Cycles*, 21, GB2015. <https://doi.org/10.1029/2006GB002784>
- 705 Takahashi, T., Olafsson, J., Goddard, J. G., Chipman, D. W., & Sutherland, S. C. (1993). Seasonal
706 variation of CO₂ and nutrients in the high-latitude surface oceans: A comparative study. *Global*
707 *Biogeochemical Cycles*, 7(4), 843–878. <https://doi.org/10.1029/93GB02263>
- 708 Takahashi, T., Sutherland, S. C., Wanninkhof, R., Sweeney, C., Feely, R. A., Chipman, D. W., et al.
709 (2009). Climatological mean and decadal change in surface ocean pCO₂, and net sea-air CO₂ flux
710 over the global oceans. *Deep Sea Research Part II: Topical Studies in Oceanography*, 56(8–10),
711 554–577. <https://doi.org/10.1016/J.DSR2.2008.12.009>
- 712 Wanninkhof, R. (2014). Relationship between wind speed and gas exchange over the ocean revisited.
713 *Limnology and Oceanography: Methods*, 12, 351–362. <https://doi.org/10.4319/lom.2014.12.351>
- 714 Wanninkhof, R., Asher, W. E., Ho, D. T., Sweeney, C., & McGillis, W. R. (2009). Advances in
715 quantifying air-sea gas exchange and environmental forcing. *Annual Review of Marine Science*,
716 1(1), 213–244. <https://doi.org/10.1146/annurev.marine.010908.163742>
- 717 Ward, B., Wanninkhof, R., McGillis, W. R., Jessup, A. T., DeGrandpre, M. D., Hare, J. E., & Edson, J.
718 B. (2004). Biases in the air-sea flux of CO₂ resulting from ocean surface temperature gradients.
719 *Journal of Geophysical Research C: Oceans*, 109(8), 1–14.
720 <https://doi.org/10.1029/2003JC001800>
- 721 Watson, A. J., Schuster, U., Shutler, J. D., Holding, T., Ashton, I. G. C., Landschützer, P., et al. (2020).
722 Revised estimates of ocean-atmosphere CO₂ flux are consistent with ocean carbon inventory.
723 *Nature Communications*, 11(1), 1–6. <https://doi.org/10.1038/s41467-020-18203-3>
- 724 Weiss, R. F. (1974). Carbon dioxide in water and seawater: the solubility of a non-ideal gas. *Marine*

725 *Chemistry*, 2(3), 203–215. [https://doi.org/10.1016/0304-4203\(74\)90015-2](https://doi.org/10.1016/0304-4203(74)90015-2)

726 Wigley, T. M. L. (1983). The pre-industrial carbon dioxide level. *Climatic Change*, 5(4), 315–320.
727 <https://doi.org/10.1007/BF02423528>

728 Woolf, D. K., Land, P. E., Shutler, J. D., Goddijn-Murphy, L. M., & Donlon, C. J. (2016). On the
729 calculation of air-sea fluxes of CO₂ in the presence of temperature and salinity gradients. *Journal*
730 *of Geophysical Research: Oceans*, 121(2), 1229–1248. <https://doi.org/10.1002/2015JC011427>

731 Woolf, D. K., Shutler, J. D., Goddijn-Murphy, L., Watson, A. J., Chapron, B., Nightingale, P. D., et al.
732 (2019). Key uncertainties in the recent air-sea flux of CO₂. *Global Biogeochemical Cycles*, 33(12),
733 1548–1563. <https://doi.org/10.1029/2018GB006041>

734 Xu, F., & Ignatov, A. (2014). In situ SST quality monitor (*iQuam*). *Journal of Atmospheric and Oceanic*
735 *Technology*, 31(1), 164–180. <https://doi.org/10.1175/JTECH-D-13-00121.1>

736 Yang, C., Leonelli, F. E., Marullo, S., Artale, V., Beggs, H., Nardelli, B. B., et al. (2021). Sea surface
737 temperature intercomparison in the framework of the copernicus climate change service (C3S).
738 *Journal of Climate*, 34(13), 5257–5283. <https://doi.org/10.1175/JCLI-D-20-0793.1>

739 Zeebe, R. E., & Wolf-Gladrow, D. (2001). *CO₂ in seawater: equilibrium, kinetics, isotopes*. Elsevier
740 Science, pp. 85–140.

741 Zhang, H., Beggs, H., Ignatov, A., & Babanin, A. V. (2020). Nighttime cool skin effect observed from
742 infrared SST autonomous radiometer (ISAR) and depth temperatures. *Journal of Atmospheric and*
743 *Oceanic Technology*, 37(1), 33–46. <https://doi.org/10.1175/JTECH-D-19-0161.1>

744

745